U(VI) speciation studies by Raman spectroscopy technique in the production of nuclear fuel

AUTHORS NAMES AND AFFILIATIONS:

Laura. J. Bonales[1,2], Nieves Rodríguez-Villagra[2]*, Iván Sánchez-García[2], Oscar. R. Montoro[3]

[1]Centro de Astrobiología (CSIC-INTA), Ctra. Ajalvir km. 4, 28850 Madrid (Spain).

[2]Centro de Investigaciones Energéticas, Medioambientales y Tecnológicas (CIEMAT). Avda. Complutense 40, 28040, Madrid (Spain).

[3]MALTA-Consolider Team, Dpto. Química Física, Facultad de Ciencias Químicas, Universidad Complutense de Madrid, 28040 Madrid (Spain).

ABSTRACT

One key intermediate solid product in the industrial production of the UO_2 for fabrication of common nuclear fuel is the ammonium diuranate or ADU. Its composition and morphology are crucial for industrial operations since this determines the quality of UO_2 powder. In this work we demonstrate that Raman spectroscopy technique is a power tool to characterize the precipitation of ADU and to monitor the precipitation reaction progress, being able to follow the U(VI) speciation and to correlate these results with the features of the obtained solid.

Thereby, here we propose the use of the Raman spectroscopy technique in the production of nuclear fuel in order to monitor the speciation of U(VI) during the ADU precipitation with dual-purpose; in one hand, to improve the safety in the fuel management and on the other hand, for the quality control for the manufacturing industry in nuclear power.

KEYWORDS: Nuclear fuel fabrication; quality control; fuel management; Ammonium diuranate; Raman spectroscopy technique, Uranium (VI) speciation.

Corresponding Author: Nieves Rodríguez-Villagra (nieves.rodriguez@ciemat.es)

Centro de Investigaciones Energéticas, Medioambientales y Tecnológicas (CIEMAT).

Avda. Complutense, 40. 28040 - Madrid (SPAIN). Tel. +34 913466290

1. INTRODUCTION

Nuclear fuel is commonly composed of ceramic UO_2 pellets, which are industrially obtained by conventional powder fabrication, consisting of pelletizing of UO_2 powder, followed by high temperature sintering in hydrogen atmosphere [1]. This process involves the generation of large quantities of UO_2 powder, and it can be obtained by dry or wet processing routes [2-6]. One of the wet chemical industrial methods for preparing UO_2 powders is the ammonium diuranate (ADU) process [7], named this way because ADU is the first intermediate in solid powder formed in the flow sheet of the UO_2 production. In this process, ADU can be precipitated from the reaction of a pure uranyl nitrate solution with ammonia (either gaseous or aqueous solution) [8, 9]. Then, the precipitate is converted first to U_3O_8, and thereafter reduced with hydrogen to UO_2 powder [1]. Thus, the ADU precipitation can be produced from uranyl nitrate and ammonium hydroxide by the following reaction [2]:

$UO_2(NO_3)_2$ (aq) + $2NH_4OH$ (aq) → $UO_3xH_2OyNH_3$ (ADU) (s) + $2NH_4NO_3$ (aq) Eq. 1

where uranyl solution reacts with ammonia and precipitation occurs when the concentration of the product (ADU) exceeds its solubility limit.

As it is described by Equation 1, the ADU stoichiometry is not constant. Therefore, the term ‘‘ammonium diuranate’’ is actually a misnomer [10], but it remains of common use. Controversies over the real composition or stoichiometry of ADU have sparked some studies [7-11] and references therein [12, 13].

The ADU composition along with its morphology is characteristics particularly important for industrial operations since, as it is well-known, these characteristics affect the desired quality of UO_2 powder obtained. For instance, the agglomeration of the ADU precipitate persists throughout calcination to U_3O_8 and the subsequent reduction to UO_2 at temperatures ~ 600 ºC [12]. Therefore, it is not surprising that a multitude of publications

dealt with the effect of different parameters that determine the ADU characteristics [13-15]. In the 1970s, Janov *et al.* [13] reported that increasing pH decreased agglomerate size. Woolfrey [14] pointed out that the thermal decomposition of ADU was affected not only by the morphology of the ADU powders, but also by its composition (ammonia and nitrate content); consequently, the rate of reduction of U_3O_8 to UO_2 increases with increasing the ammonia content. In a more recent study, Murty *et al*. [15] have shown the influence of the temperature on the growth rate and particle size of the ammonium diuranate powder. Low temperatures lead to low precipitation rates, which favor the dispersion of the precipitated particles (smaller agglomerates size) and therefore, preferred in view of the sinterability requirement of the final uranium dioxide powders. Moreover, in the last few years, some authors have tried to analyze the progress of the ADU precipitation [16, 17]. These authors study the reaction of uranyl nitrate and ammonia. Paik *et al.* [17] investigated the effect of ammonium nitrate concentration on ADU precipitation, finding that as the time and the excess ammonium nitrate increase, the pH also increases, leading to the formation of more number of phases and more agglomerates, in agreement with the study shown by Janov *et al*. [13]. A similar result was found by Manna et al. [16], who observed that ADU produced with aqueous ammonia was denser than ADU performed with gaseous ammonia. In all of these studies, the ADU precipitate was the main focus of the research, but not in the uranyl solution. The speciation of U(VI) as the progress of the ADU precipitation was not the focus of these mentioned studies. This speciation must be directly related to the precipitation mechanism and then to the different ADU particles obtained, as Tomazic et *al.* [18] assumed more than 40 years ago. These authors proposed the presence of anionic uranyl hydroxo complexes on ADU precipitation at alkaline pH.

Uranyl speciation as a function of pH has been studied from the 1980s by using Raman Spectroscopy technique (RS), and more recently by Müller *et al.* [19] using Attenuated Total Reflection Fourier-transform infrared- ATR FT-IR. Toth and Begun [20] measured the Raman spectra of UO_2^{2+} ion as a function of pH adjusted with HNO_3 and NaOH solutions and identifying the ions: UO_2^{2+}, $(UO_2)_2$ $(OH)_2^{2+}$, and $(UO_2)_3$ $(OH)_5^{+}$ with the different symmetric stretching band, v_1 as a fingerprint. Several works can be found concerning the speciation of uranyl ion using RS; Brooker *et al.* [21] noted that the stretching modes of monodentate and bidentate nitrate to the uranyl cation could be differentiated; Maya and Begun [22] studied the stability of the uranyl ion in the presence of carbonate; Trung *et al.* [23] in a variety of inorganic and organic ligands and Dargent *et al.* [24] studied the uranyl-chloride complex under hydrothermal conditions. In addition, the feasibility of RS for the estimation of the relative abundance of uranyl species over the pH range relevant to ADU precipitation has been established [25,26]. None of the above mentioned works were particularly focused on ADU precipitation reaction.

In this work, the use of the Raman spectroscopy technique is proposed for tracking the ADU precipitation from a $UO_2(NO_3)_2$ solution, by adding different quantities of NH_4OH solution throughout the pH range from ~2 to ~9 in ambient atmosphere. Special attention is focused not only on the characteristics of the obtained ADU, but also on the quantification and speciation of U(VI) during the reaction progress related to the ADU precipitate characteristics.

2. EXPERIMENTAL PART

2.1. Chemicals

Aqueous solutions were prepared using ultra-pure Milli-Q water (Millipore, 18.2 MΩ·cm from a MilliPore ELIX system) with TOC (Total Organic Carbon) lower than 5–10 ppb. Uranyl nitrate hexahydrate, $UO_2(NO_3)_2 \cdot 6H_2O$, was supplied by Fluka and ammonium hydroxide (NH_4OH, 30%) from Panreac, and both are used without further purification. The sample preparations and analysis were run under ambient conditions.

2.2. Characterization techniques

Raman spectrometer

Raman spectra were acquired by using a Horiba LabRam HR evolution spectrometer (Jobin Yvon Technology). The 532 nm laser beam (nominal power 50 mW) was focused onto the sample through the 5x or 100x objectives, for liquid and solid samples respectively, of an Olympus BX41 microscope. The scattered radiation was then collected in backscattering geometry, dispersed using a 600 grooves/mm holographic grating and recorded by a CCD detector (256 x 1024 pixels). The resolution of the instrument was better than 0.48 cm^{-1}/pixel. For the analysis of aqueous solutions, small aliquots were housed in a home-made cuvette designed to measure liquid samples (a more detailed description can be found elsewhere [27]). A typical spectrum from 400 to 4000 cm^{-1} range was obtained within 4-5 seconds of acquisition time and 10 accumulations for solid samples and 60 seconds of acquisition time and 3 accumulations for liquid samples. All acquired spectra were recalibrated using a Neon emission light. The excitation laser power was minimized to 1 mW to prevent the alteration of the solid samples. For the

analysis of each sample, the average of 8 spectra recorded at different locations was acquired over the wavenumber range from 400 to 1560 cm^{-1}.

X- Ray diffractometer

XRD characterization was performed by means of a Philips PANalytical X'Pert MPD diffractometer using Cu Kα1 radiation (l = 1.54056 Å) and operating at 45 kV and 40 mA. A Bragg– Brentano configuration geometry was used. The 2θ range covered was from 20^o to 120^o at 0.04^o scanning steps.

Complementary techniques

Inductively Coupled Plasma - Quadrupole Mass Spectrometry ICP-MS, Thermo Fischer Sci ICAP-Qc model with collision cell (QCell) and KED mode (He- Kinetic Energy Discrimination), were used in order to analyses the total U content of the aqueous samples. A DuoPUR acid purification system (Milestone) was used for guaranteed reagent further purification of HNO_3 (65%). A standard uranium solution 100 µg/mL (Inorganic Ventures, MSU, 99.98% of purity) was used for preparation of eight concentration levels (0, 0.05, 0.1, 0.5, 1, 5, 10, and 50 µg/L), which were used for establishing calibration curves to determine the unknown [U]. The standard stock solution of ^{193}Ir (1000 µg/mL; Merck) was used for the preparation of 100 µg/L internal standard solution. Instrumental operating parameters were optimized using a 1 µg/L ICP multi-element standard solution (Tune B, Thermo Fischer) containing Ba, Bi, Ce, Co, In, Li and U. All standards were used without further purification and prepared in 2% (v/v) HNO_3. The solution pH was measured using a pH meter Metrohm 808 Titrando with a pH Glass Electrode (Metrohm). The pH electrode was calibrated with commercial pH buffer solutions (Reagecon pH 4 and 7).

The ADU precipitated surface morphology has been examined by means of a TM4000 Plus SEM by HITACHI, using a working voltage of 15 kV. The microscope is equipped with a Back-Scattering Electrons (BSE) detector, which provides clear images about powder surfaces, and a Secondary Electrons (SE) detector, which gives information about the relief of the surfaces.

2.3. ADU precipitation procedure

ADU precipitation reactions were carried out by adding dropwise different aliquots of 0.442 M NH_4OH to a fixed sample volume of 500 µL of uranyl nitrate solution, 0.251 M $UO_2(NO_3)_2$ in individual batch tubes (BRAND®, PP) with a total volume of 2 mL (see Table 1). The reaction was performed on uranyl nitrate solutions resulting from sample 1 (25µL of ammonia addition) to sample 12 (maximum concentration achieved of NH_4OH), in a gradual flocculation of a dense yellow phase (Figure 1). After waiting 15-20 min and shaking each batch solution for 5 min with a Vibromatic shaker, the solid was separated from the supernatant by filtration using ultracentrifugation (Amicon Ultra-4 3k Centrifugal Filter, Millipore 1 - 2 nm) for 60 min. The filtered ADU was naturally dried at ambient conditions. Aliquots of each batch solution were taken for: i) elemental analysis with ICP-MS to determine the U total concentration at each addition of ammonia in the filtrate, ii) Raman spectra measurements for U-speciation in solution and iii) pH measurements in the filtrate. The collected ADU powder was characterized by XRD, RS and SEM techniques.

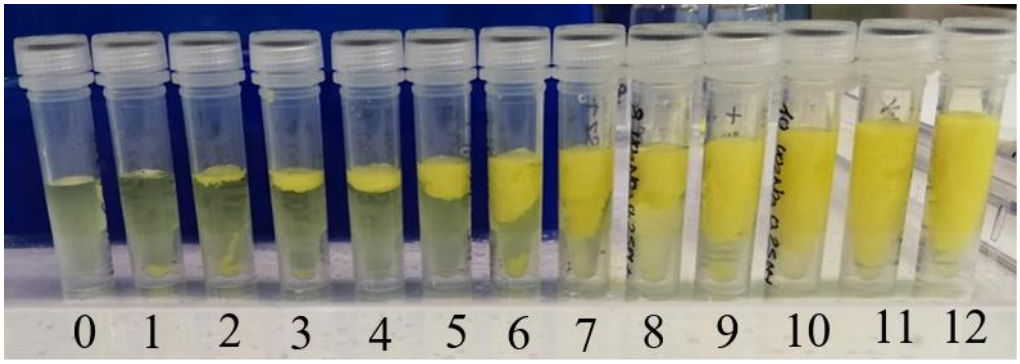

Figure 1. Photograph of precipitation reaction containing an initial volume of 500 μL 0.251 M $UO_2(NO_3)_2$ and progressively increase of solution of 0.442 M NH_4OH.

Table 1. Volume of solution of 0.442 M NH_4OH added to a 0.251 M $UO_2(NO_3)_2$ solution of 500 μL in each batch reactions, pH and NH_4^+/ U^{6+} ratio. (* $[NH_4^+]_{theor}$ /$[U^{6+}]_{ICP-MS}$ values were obtained by calculating the NH_4^+ concentration theoretically, whereas the $[U^{6+}]$ was quantified by ICP-MS by withdrawing a liquid aliquot of each sample, and after being conditioned with 10% HNO_3 solution)

Batch sample ID	***Volume of NH_4OH added/ μL***	***pH***	***$[NH_4^+]_{theor}$ / $[U^{6+}]_{ICP-MS}$ Ratio****
0	0	1.99	0.0
1	25	2.46	0.1
2	50	2.55	0.2
3	75	2.65	0.3
4	100	3.03	0.3
5	150	3.33	0.6
6	200	3.44	1.0
7	250	3.62	1.7
8	300	3.88	3.4
9	350	6.36	8.6
10	400	8.26	8.5
11	450	8.68	9.6
12	500	8.93	11.2

3. RESULTS

3.1. Analysis of uranyl nitrate solutions as a function of NH_4OH added

Determination of U concentration

Changes in the U^{6+} concentration were monitored for each batch solution by ICP-MS and RS. Uranium concentrations measured by ICP-MS *vs.* pH in the filtered yellow solutions are plotted in Figure 2. Concentration errors were calculated by multiplying RDS (relative to measured concentration values) by a coverage factor of 95%. In this figure, two inflection points were observed (see vertical lines) leading to three regions: firstly, a gradual decrease of measured uranium concentration with pH up to sample 4 (100 µL, pH ~3); a sharp decrease (up to pH ~3.9), and a third and final region, from sample 9 (350 µL, pH ~6.4), where a complete uranyl precipitation is achieved.

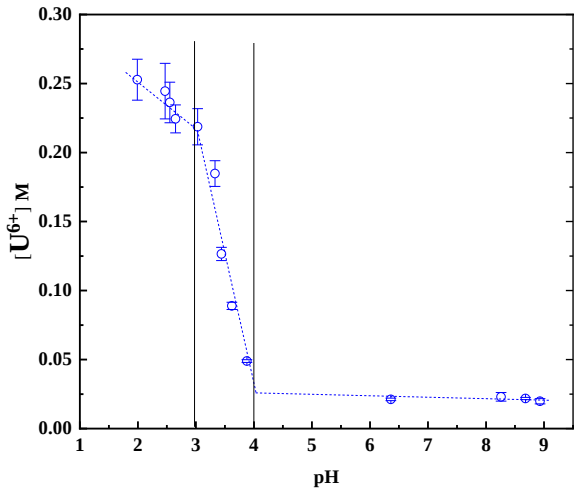

Figure 2. Uranium concentration (filtered) as a function of pH resulting from the 0.442 M NH_4OH addition to uranyl nitrate solutions. Dot lines indicate visual guides.

The reactions were also studied by measuring the decrease in the concentration of the uranyl and nitrate ions in the supernatant of each aqueous batch solution by using

quantitative Raman spectroscopy (QRS) [28, 29]. For this purpose, a series of $UO_2(NO_3)_2$ (*aq*.) Raman spectra were collected from solutions at the following concentrations: 0, 0.025, 0.05, 0.10, 0.15, 0.20, and 0.25 M, in the 400–4000 cm^{-1} wavenumber spectral range, see Figure 3.A. Note that all spectra were normalized with the isosbestic point of water located at 3468 cm^{-1} [30].

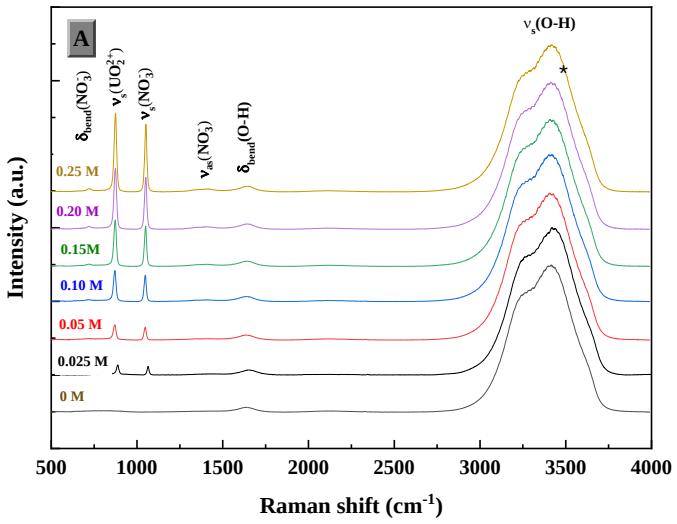

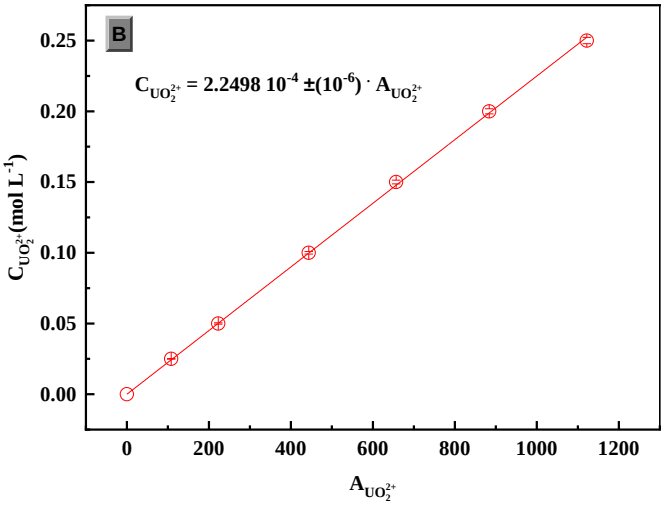

Figure 3. A) Raman spectra of $UO_2(NO_3)_2$ (aq.) solution at concentration of 0, 0.025, 0.05, 0.10, 0.15, 0.20, and 0.25 M. The asterisk indicates the isosbestic point of water located at 3468 cm^{-1}. **B)** Calibration curve of uranyl ion.

In Figure 3.A, the assignation of the main bands is indicated as following:

- Broad bands at high frequencies (2800–3400 cm^{-1}) correspond to the OH-bond stretching, ν_s(O-H) [31] and the band at ~1630 cm^{-1} to the OH bending, δ_{bend}(O-H) [31].
- The intense narrow band at ~ 874 cm^{-1} has been assigned to the uranyl stretching symmetric vibration, $\nu_s(UO_2^{2+})$ [20].
- The band at ~708 cm^{-1} corresponds to the in plane deformation of the NO_3^-, $\delta_{bend}(NO_3^-)$ [32]; the intense band located at around 1037 cm^{-1} corresponds to the N-O stretching of the NO_3^- ion, $\nu_s(NO_3^-)$ [33]; and the broad bands at ~1400 cm^{-1} are assigned to the asymmetric stretching bands of the nitrate ion, $\nu_{as}(NO_3^-)$ [32].

As can be seen, as the concentration of the uranyl nitrate increases, spectra do not present any new Raman bands and the relative intensity of the bands keeps constant. Brooker *et al.* [21] found different behavior because the concentration range was distinct, *i.e.*, up to 2.29 M, being the most concentrated solution in this study 0.25 M. Since these peaks do not overlap, Raman analysis of the integrated intensity gives us a measure of the concentration by the construction of a calibration curve (see Figure 3.B) [27].

Figure 4 shows the obtained Raman spectra of each batch. As can be appreciated, a new band appears as a shoulder at ~853 cm^{-1} (see asterisk in Figure 4.A) in the first addition (25μL). Henceforth and up to 150 μL, the intensity of such additional band increases, whereas the band at ~ 875 cm^{-1} $\nu_s(UO_2^{2+})$ decreases. From this added volume on, both bands decrease until they vanish at ~ 350 – 500 μL (Figure 4.B and C). This fact agreed with the flat zone of uranium concentration in solution quantified by ICP-MS (see Figure 2). The new band at ~ 853 cm^{-1} also corresponds to the symmetric vibration to the uranyl ion, $\nu_s(UO_2^{2+})$, as was addressed by Toth and Begun [20], who first observed a redshift as the pH increases by the NaOH addition to a uranyl aqueous solution. The shift of this

band indicates a different environment of the uranyl ion, *i.e.* distinct speciation/complexation.

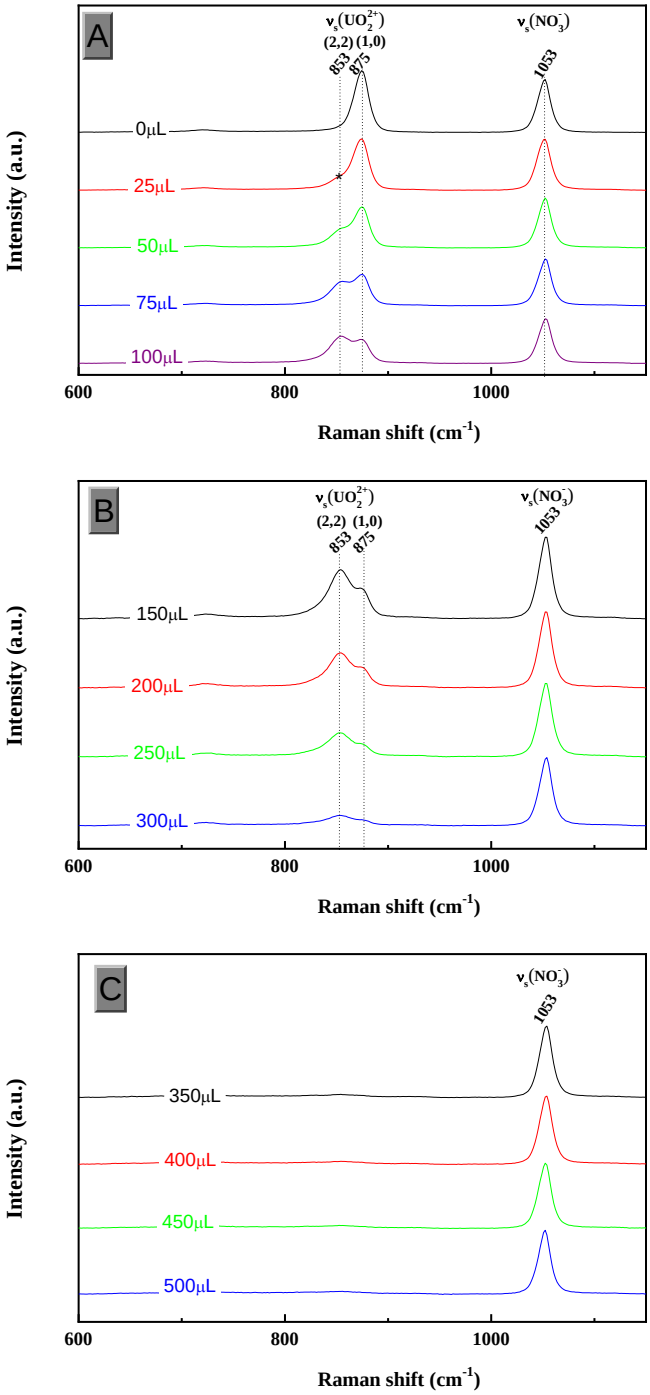

Figure 4. Raman spectra of each batch reaction (see Table 1) of the clear supernatant liquid. Fig. 4.**A** shows the spectra obtained after the addition up to 100 µL of NH_4OH (pH ~ 3). Spectra corresponding to the addition up to 300 µL (pH from 3.3 to 3.9) and up to 500 µL (pH from 6.4 to 8.9) are shown in Figures 4.**B** and 4.**C** respectively**.**

Quiles and Burneau [25] have described this behavior due to the formation of hydroxo complexes with a stoichiometric coefficient *(x,y)* formed as a function of pH by the known reaction (Eq. 2):

$$x UO_2^{2+} (aq) + y\ H_2O \rightarrow (UO_2)_x\ (OH)_y^{(2x-y)+} (aq) + y H^+ (aq). \quad \text{Eq. 2}$$

These authors found the Raman shift, 870, 853, and 835 cm^{-1} for the complex with a stoichiometric coefficient *(1,0)*, *(2,2)*, and *(3,5)* respectively. Note that the hydrated uranyl ion, written UO_2^{2+} for simplicity, is then named *(1,0)* and is considered as ''uncomplexed'' in water. The different values observed in the $\nu_s(UO_2^{2+})$ are directly related to the strengthening/weakening of the U-O bond. Thus, the increase in the Raman wavenumber reveals a stronger U-O bond, with a shorter length [34]. Thereupon, the U-O distance increases for the different ions as the ratio of the stoichiometric coefficient x/y, increases, (1,0) > (2,2) > (3,5). As a first approach, we have tentatively assigned the $\nu_s(UO_2^{2+})$ at ~ 875 cm^{-1} to the free ion in the complex *(1,0)*, and the one at *ca.* 853 cm^{-1} to the ion in the complex *(2,2)*, $(UO_2)_2\ (OH)_2^{2+}$. Assuming this assignation, the overall changes observed in Figure 4 indicates that as the amount of NH_4OH added increases up to 150 µL, the complex *(1,0)* decreases and the *(2,2)* complex increases; then both decrease until the uranyl ion concentration is negligible.

3.2. Elemental analysis vs QRS of uranyl nitrate solutions. Solution speciation

The concentration of *(1,0)* complex can be calculated in a straightforward manner from the calibration curve obtained from spectra shown in Figure 4. For the *(2,2)* complex analysis, the same calibration curve was applied by assuming that the molar scattering coefficient of the $\nu_s(UO_2^{2+})$ remained unchanged regardless of its complexation, as was highlighted in [25]. To test this hypothesis, we compared the uranyl ion total concentration obtained by QRS, $[U^{6+}]_{QRS}$ *vs.* the total U(VI) concentration obtained by ICP-MS, $[U^{6+}]_{ICP\text{-}MS}$ in solution after each ammonia addition. Each data point is for a

single measurement. This comparison from both approaches is shown in Figure 5. The result adjusts to a linear correlation function of slope =1.09 ± (0.01) with a coefficient of determination (R^2) equal to 0.998 and Pearson's R =0.999. This result verifies that the molar scattering coefficient does not change for the two uranyl ions, *(1,0)* and *(2,2)* and therefore, it is possible to calculate the uranyl concentrations ions by using the same calibration curve.

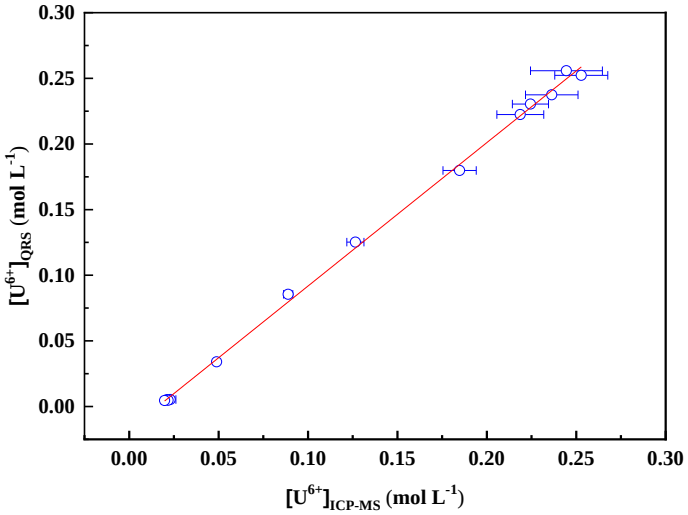

Figure 5. Correlation of the uranyl concentration dataset obtained by QRS and by using ICP-MS.

Figure 6 shows the obtained concentrations of uranyl ions as a function of the NH_4OH addition to a uranyl solution of 0.251 M. As it can be seen, the concentration of UO_2^{2+} ion decreases continuously, whereas $(UO_2)_2(OH)_2^{2+}$ concentration increases up to a maximum and then decreases. Figure 6 has been divided into three regions, region A, from 0 to 100 µL, in which the $[UO_2^{2+} \geq [(UO_2)_2(OH)_2^{2+}]$, at 100 µL, $[UO_2^{2+}]$ $=[(UO_2)_2(OH)_2^{2+}]$ =0.11 M; region B from 100 to 350 µL, in which the $[UO_2^{2+} \leq$ $[(UO_2)^2(OH)_2^{2+}]$, and region C, at volume addition > 350 µL, where $[UO_2^{2+}]$ and $[(UO_2)_2(OH)_2^{2+}]$ are very low.

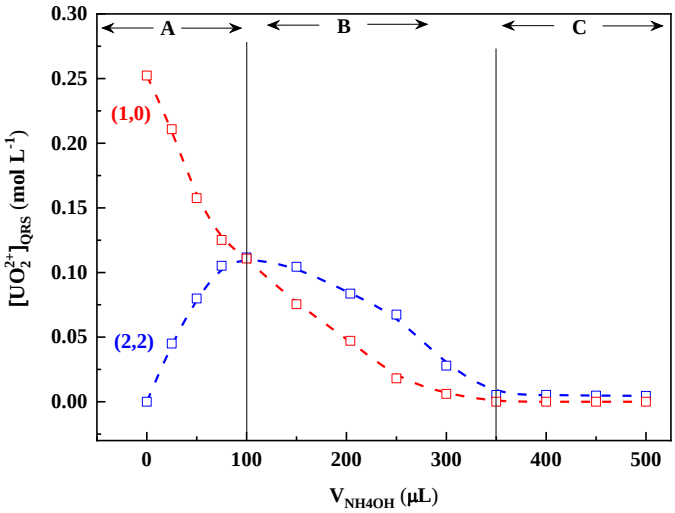

Figure 6. Concentration of uranyl ions as a function of the added volume of NH_4OH. (1,0) complex indicates the UO_2^{2+} ion and (2,2) indicates the$(UO_2)_2(OH)_2^{2+}$ ion.

Once we had analyzed this general behavior, we performed a reliable QRS analysis to obtain (*i*) the concentration of each uranyl ion and (*ii*) the concentration of uranyl precipitated, both as a function of the NH_4OH addition and pH. Quantification of the relative abundance of each ion and the amount of precipitate formed as a function of pH have been calculated as a molar fraction from the data shown in Figure 6. This representation is observed in Figure 7 where *n(1,0)* is the molar fraction of the complex UO_2^{2+} calculated as (nUO_2^{2+}*/n(total))100; n(2,2)* is the molar fraction of the complex $(UO_2)_2(OH)_2^{2+}$ and it was calculated as *($nUO_2(OH)_2^{2+}$/n(total))·100,* and *nADU* is referred to the molar fraction of the precipitated calculated as *n(total) - n(1,0) -n (2,2).* In this figure, we have also stated by vertical lines the regions mentioned in Figure 6. For the sake of comparison, the effect of the addition of NaOH and NH_4OH in the presence of the different species, can be observed. Figure 7.A shows the well-known phase diagram reproduced from ref. [20], whereas in Figure 7.B is represented the empirical phase diagram obtained in this work. From this comparison, it is apparent that the distribution of uranyl ions is very similar in both systems, *i.e.*

- At pH ~ 3.5 (3.8 for NaOH and 3.3 NH_4OH), the *(2,2)* compound, when complex reaches its maximum concentration, is the dominant species (~ 60% for NaOH and 55% for NH_4OH).
- At pH > 3.5, *(1,0)* and *(2,2)* complexes decreases. But more important regarding the precipitation of ADU are the found similitudes between the complex *n(3,5)* and the *n(ADU)*, both increases exponentially from pH > 3 (pH =3.2 for NaOH and pH=3.0 for NH_4OH), reaching maximum values at around pH ~ 5-6. For NaOH at pH > 5.5, the *(3,5)* complex dominates at 100%, whereas at pH > 6 in the NH_4OH reaction studied, we found 96 % of ADU precipitated and less than 4 % of *(2,2)* complex in the supernatant solution.

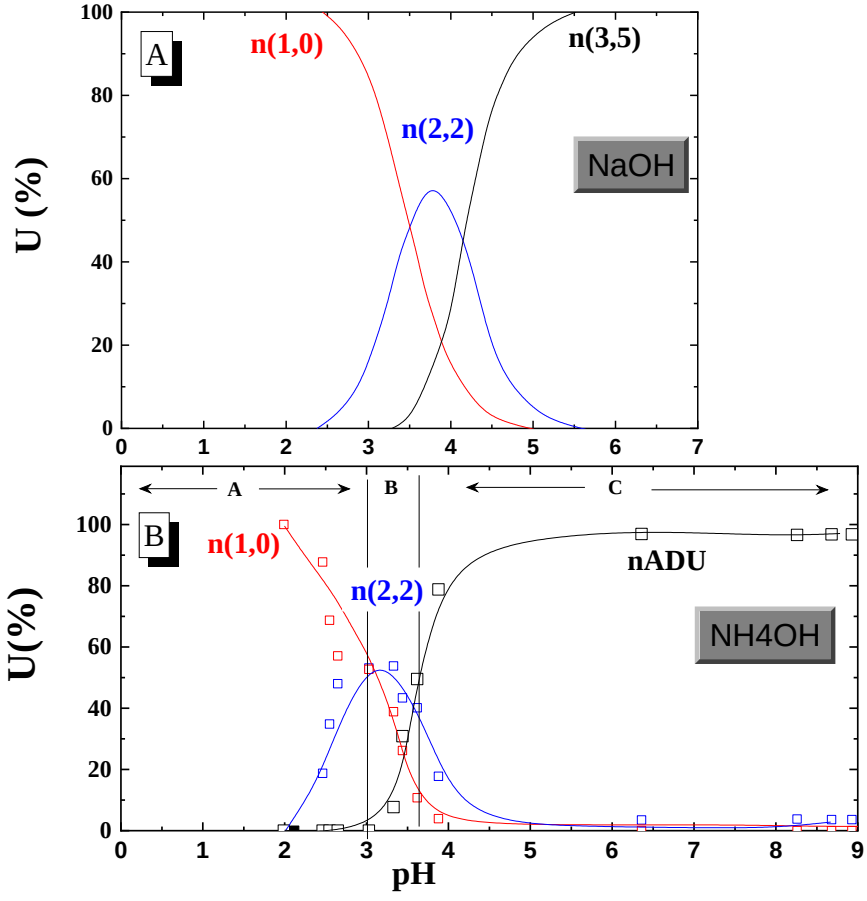

Figure 7. Uranium (VI) speciation diagrams as a function of pH: A) by adding NaOH (upper graph, reproduced from [20]) and B) by adding NH_4OH (bottom graph) from this work. Color lines in the bottom graph are visual guides.

3.3. Solid phase identification

After the precipitation reaction of the different batch, we filtered the supernatant and selected several crystal specimens for molecular analysis by SEM (Figure 8), XRD and RS (Figure 9.A. and 9.B.), respectively. At the first addition, the solution became turbid and a yellow gelatinous phase was detected. In the first four samples, the amount of colloidal particles was quantitatively low, being impossible to be recovered from the ultrafilters. No particular differences were found in the yellowish color of the ADU samples.

Morphological analysis

Representative SEM images acquired for these samples can be seen in Figure 8. In general, clumped massive agglomerates with a wide range of submicron particle were found across the larger compacted solids at all pH range evaluated. The micro- and nano-spherical particles displayed very similar morphologies consisting of a rounded habit arranged in irregular clumps. Overall, in the qualitative morphological characterization in this study, any readily identifiable difference in the resulting products as a function of the pH was identified, exhibiting identical shape.

Our main conclusion from these images is that the higher the pH of the ammonium diuranate precipitated, the higher the dispersion of size range of the agglomerates were obtained, which may affect the final densities of sintered pellets. In addition, higher pH (*i.e.* from pH ~ 8.6) leads to lower primary agglomerates size, as expected, which would be undesirable, keeping in mind sinterability specifications of final UO_2 powder.

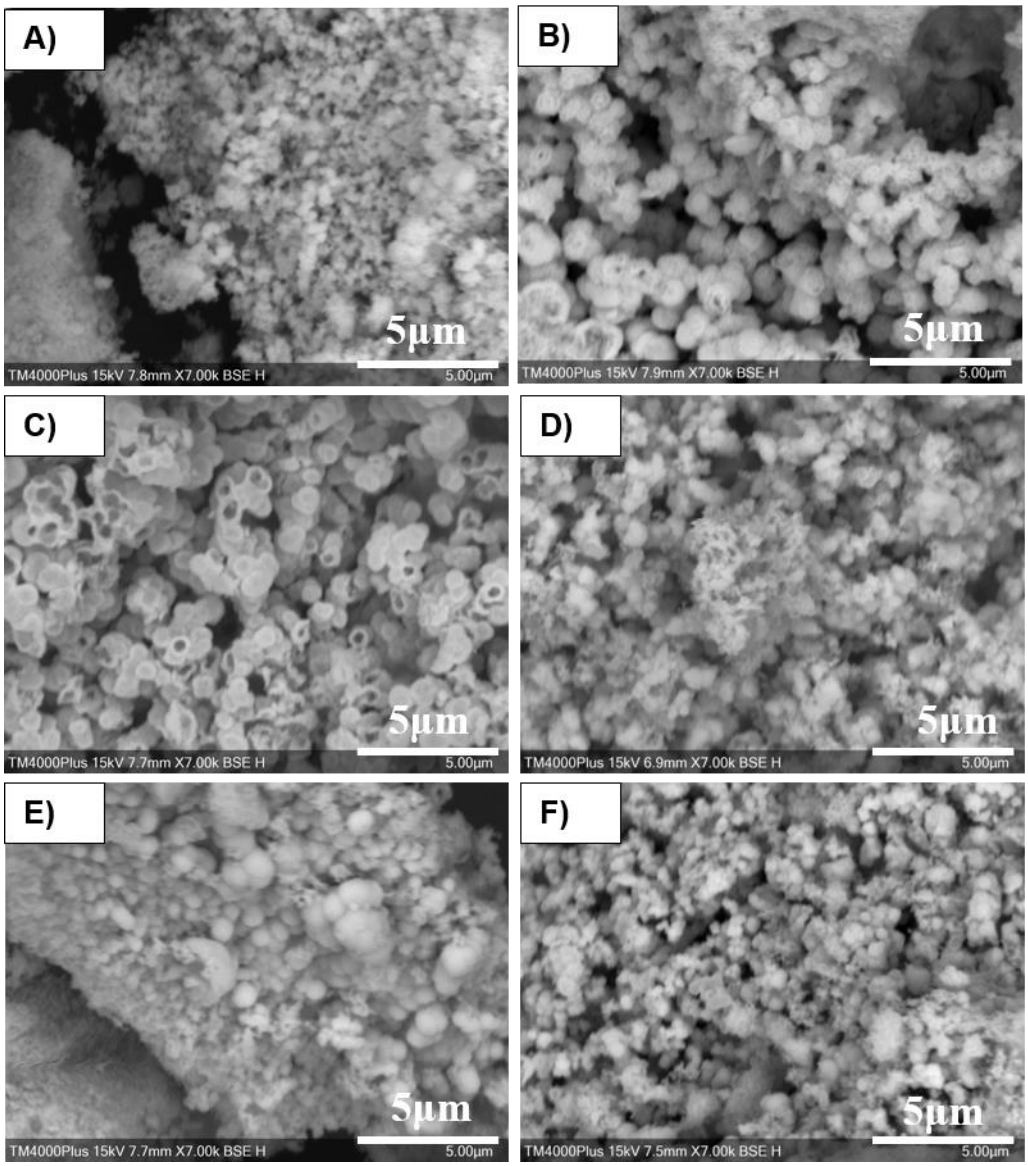

Figure 8. Representative SEM images of ADU powder particle precipitated at increasing amounts of NH_4OH added (pH 3 to 8.9) to constant uranyl nitrate solution of each solid obtained. Spheroidal type forms are shown from all ADU identified: A) ADU-4 (100 µL of 0.251 M $UO_2(NO_3)_2$) and pH = 3.03; B) ADU-7 (250 µL of 0.251 M $UO_2(NO_3)_2$) and pH = 3.62; C) ADU-8 (300 µL of 0.251 M $UO_2(NO_3)_2$) and pH = 3.88; D) ADU-9 (350 µL of 0.251 M $UO_2(NO_3)_2$) and pH = 6.36; E) ADU-10 (400 µL of 0.251 M $UO_2(NO_3)_2$) and pH = 8.26; F) ADU-12 (500 µL of 0.251 M $UO_2(NO_3)_2$) and pH = 8.93. Note that it is the same scale for images.

XRD analysis

Regarding the XRD diffractograms shown in Figure 9.A, a peak broadening was observed at pH 3.88 (300 µL NH_4OH) resembling an amorphous phase (considerably more pronounced at higher pHs), in contrast with well-defined Bragg peaks in X-ray diffraction of ideal crystalline substances [35]. Although this fact obscures a reliable quantitative analysis of the precipitates, it is possible to determine that ADU precipitated at higher pH contains more amount of ammonia than ADU precipitated at acidic conditions due to the fact that the crystallinity of ADU decreases markedly with increasing the ammonia content, as indicated by Debets and Loopstra [36]. It is noteworthy that the four existing compounds in the system NH_3-UO_3-H_2O were well defined by Cordfunke in 1962 [37] and its corresponding X-ray power diagrams were indexed a year later by Debets and Loopstra [36]. Thereby, the formulae of these compounds are: (I) UO_3 $2H_2O$, (II) $3UO_3$ NH_3 $5H_2O$, (III) $2UO_3$ NH_3 $3H_2O$ and (IV) $3UO_3$ $2NH_3$ $4H_2O$ being the first two compounds orthorhombic and the two latter hexagonal.

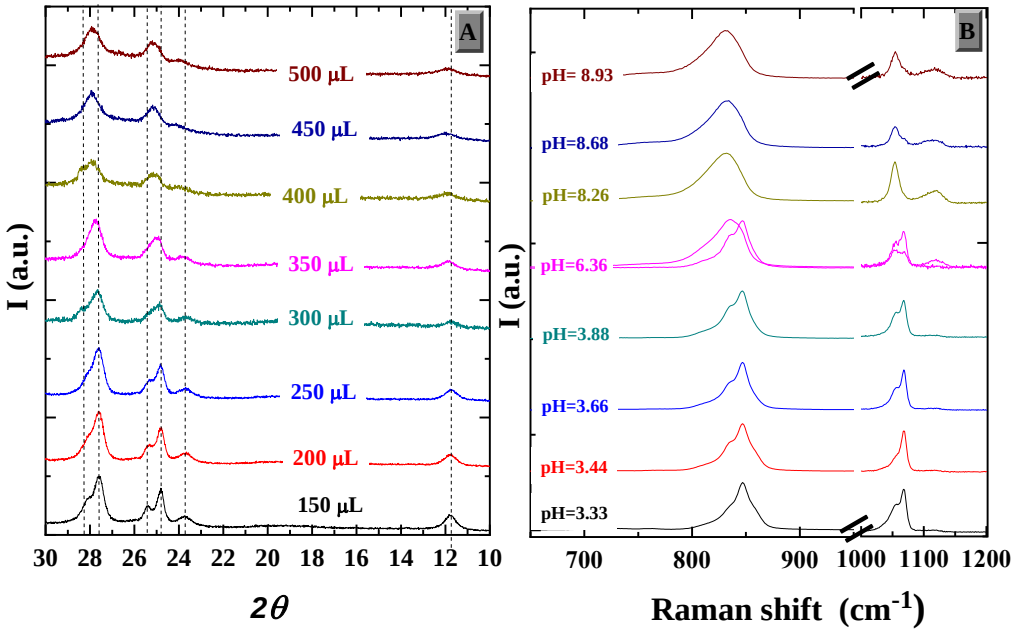

Figure 9. XRD diffractograms (A) and Raman spectra (B) of each solid obtained in batch from 5 to 12.

A qualitative analysis was carried out by comparing the diffractograms of the precipitated compounds with the diffraction pattern published by Debets and Loopstra [36]. The ADU obtained in this work can be described by the combination of the compounds (II) $3UO_3$ NH_3 $5H_2O$ and (III) $2UO_3$ NH_3 $3H_2O$, in agreement with the results shown by Paik *et al.* [17]. As an example, Figure 10 shows the XRD analysis profile of the ADU compounds prepared by adding a volume of 150 and 500 µL of NH_4OH at acidic and basic pH, respectively.

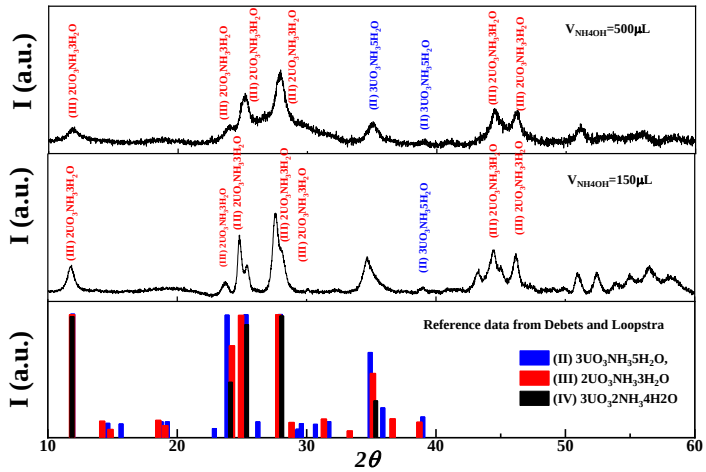

Figure 10. XRD analysis profile of the ADU compounds prepared by adding a volume of 150 and 500 µL of NH_4OH to a 0.251 M $UO_2(NO_3)_2$ solution.

Raman analysis

In Figure 9.B, it becomes clear that two different Raman spectra patterns can be distinguished: one pattern from a NH_4OH volume addition from 150 up to 350 µL and another up to a volume > 350 µL. It should be noted that these volume ranges correspond to the regions B and C, respectively, of the uranium (VI) speciation diagram (Figure 7.B). Therefore, the solid precipitated from the solution in region B and C is now called ADU_B and ADU_C, respectively. It is noteworthy that close to neutral pH ~6.36, corresponding to the 350 µL addition, we have obtained a mixture between the two mentioned patterns

in the RS analysis. The Raman spectra of this sample have been acquired at different locations, and both patterns corresponding to the ADU_B and ADU_C were found. Thus, the Raman spectra shown in this figure corresponds to the average of the acquired spectra separately, whereas the others are the average of the total spectra obtained in each sample. As opposed to the detailed knowledge of the XRD corresponding to the existing compounds in the system NH_3-UO_3-H_2O, no previous data of Raman spectra related to its stoichiometry or composition exist, as far as we know. In Figure 11 (K and L), Raman spectra of the precipitated ADU_B and ADU_C are compared with some of the ones found in literature (Figure 11.A-J). The inconsistency of the Raman data reflected in Figure 11 is presumably due to the fact that authors referred ADU or even yellowcake to different mentioned solids in the system UO_3-NH_3-H_2O. Thus, the Raman spectra reported in previous studies do not determine the specific composition, either an assignation of each band, with the exception of uranyl symmetric bands. Symmetric stretches of UO_2^{2+} ion, which are observed in multiple U-bearing minerals [38], are found in the region of 750-900 cm^{-1}. This band has been traditionally used as a fingerprint of most of them [39], *i.e.*, this band appears at *ca*. 750-850 cm^{-1} for uranyl in the system NH_3-UO_3-H_2O. Besides, it can be observed the $\nu_s(UO_2^{2+})$ in a few cases shows an internal structure of several very closely spaced sub-peaks, which most likely pointed to a varying environment around the uranyl ion within the same material.

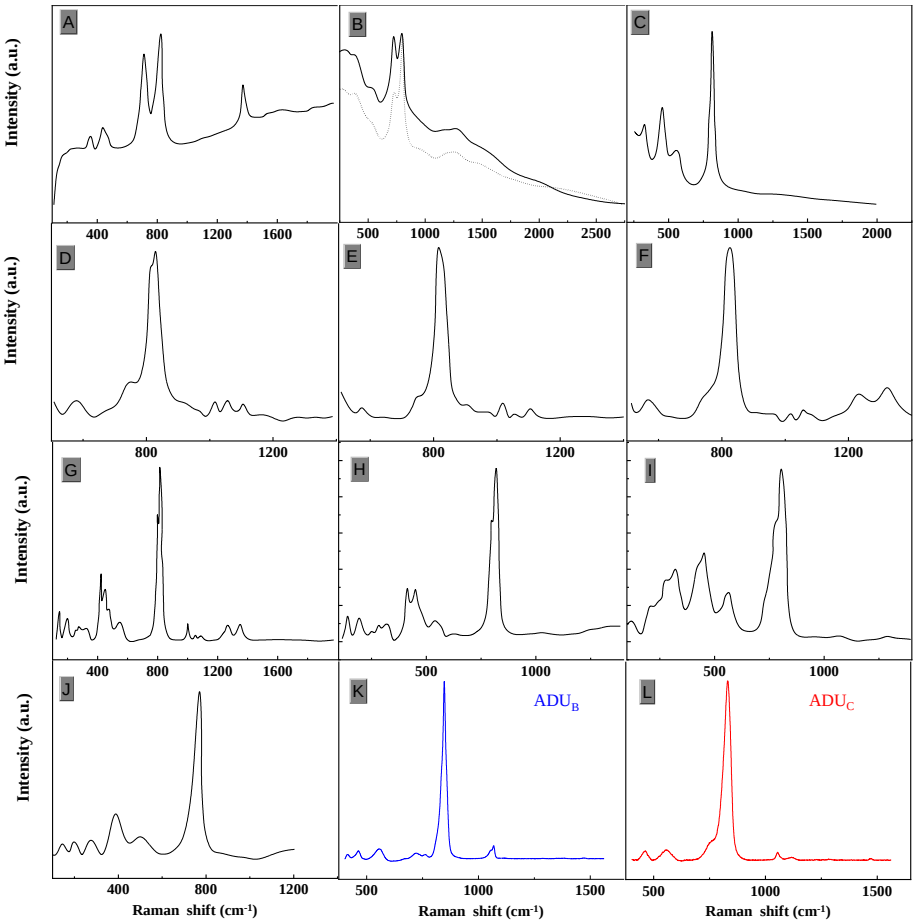

Figure 11. Raman spectra of several ADU precipitated: **A)** reproduced from ref [40]; **B)** reproduced from ref. [41] where straight line corresponds to powder and dot line to the pellet; **C)** synthetic ADU from ref. [42] , **D), E)** and **F)** reproduced from ref C, corresponds to natural samples: Ellweiler, Brunhilde and Dawn location respectively; **G)** reproduced from ref [43]; **H), I)** and **J)** are reproduced from [44] and correspond to natural samples from Millken lake, El Dorado and Dellf; **K)** and **L)** are the spectra obtained in this work from the acidic and alkali solutions, *i.e.* ADU_{acidic} and ADU_{alkali}, respectively.

Although only a qualitative analysis of the ADU has been achievable to attain by XRD technique, it is possible, however, to carry out a detailed analysis for the obtained Raman data. For this aim, the measured spectra were subjected to the second derivative, *i.e.* the frequency of a given band corresponds to a minimum in the second derivative function.

A detailed band-profile analysis of the spectra was then accomplished by performing multi-band Voigt profiles fitting, with the frequencies of each band obtained in the second derivative analysis as fixed parameters (see Table S1 at the supplementary information). An example of the profile analysis is given in Figure 12. As Figure 12 illustrates, main band $\nu_s(UO_2^{2+})$ exhibits an internal structure composed of 4 main contributions. The respective peaks of the ADU_B solids (from 100 μL to 350 μL, and pH< 6.33) are centered at *ca*. 824, 836, 847 and 855 cm^{-1}. For the named ADU_C precipitate, the contribution bands are located at 758, 811, 836 and 847 cm^{-1}, that is, two new bands at low frequency take shape (758 and 811 cm^{-1}), and the higher frequency band at ~855 cm^{-1} disappears, while bands at ~836 and 847cm^{-1} also contribute to the band profile of these ADU_C solid. As mentioned in above, the changes in these $\nu_s(UO_2^{2+})$ are directly attributed to the strengthening/weakening of the U-O bond. Thereupon, the bands at a higher frequency in the ADU_B indicate an increase in the U-O length of the uranyl ion, whereas, in comparison to the ADU_C structure, the lower frequency reveals a weaker U-O bond, with a shorter length.

The decreases in the frequency have been analyzed by Infrared spectroscopy by Stuart and Whateley [10]. These authors highlighted that the uranyl ion frequency decreases with increasing the NH_4^+ content, *i.e*. the U-O bond length is greater for ADU with higher ammonia amount, indicating that ADU_C has more NH_4^+ than ADU_B. These outcomes are in agreement with the ones obtained in the XRD analysis. Thus, jointly considering the results of Raman and XRD analysis, ADU_B and ADU_C can be attributed to a mixture of (II) $3UO_3\ NH_3\ 5H_2O$, (III) $2UO_3\ NH_3\ 3H_2O$, where the compound (III) with higher content in NH_4^+ prevails in ADU_C more than in ADU_B.

The empirical equation published by Bartlett and Cooney [45] was applied in order to quantify the U-O bond lengths from the uranyl symmetric stretching frequencies. The resulting bond lengths are given in Table 2.

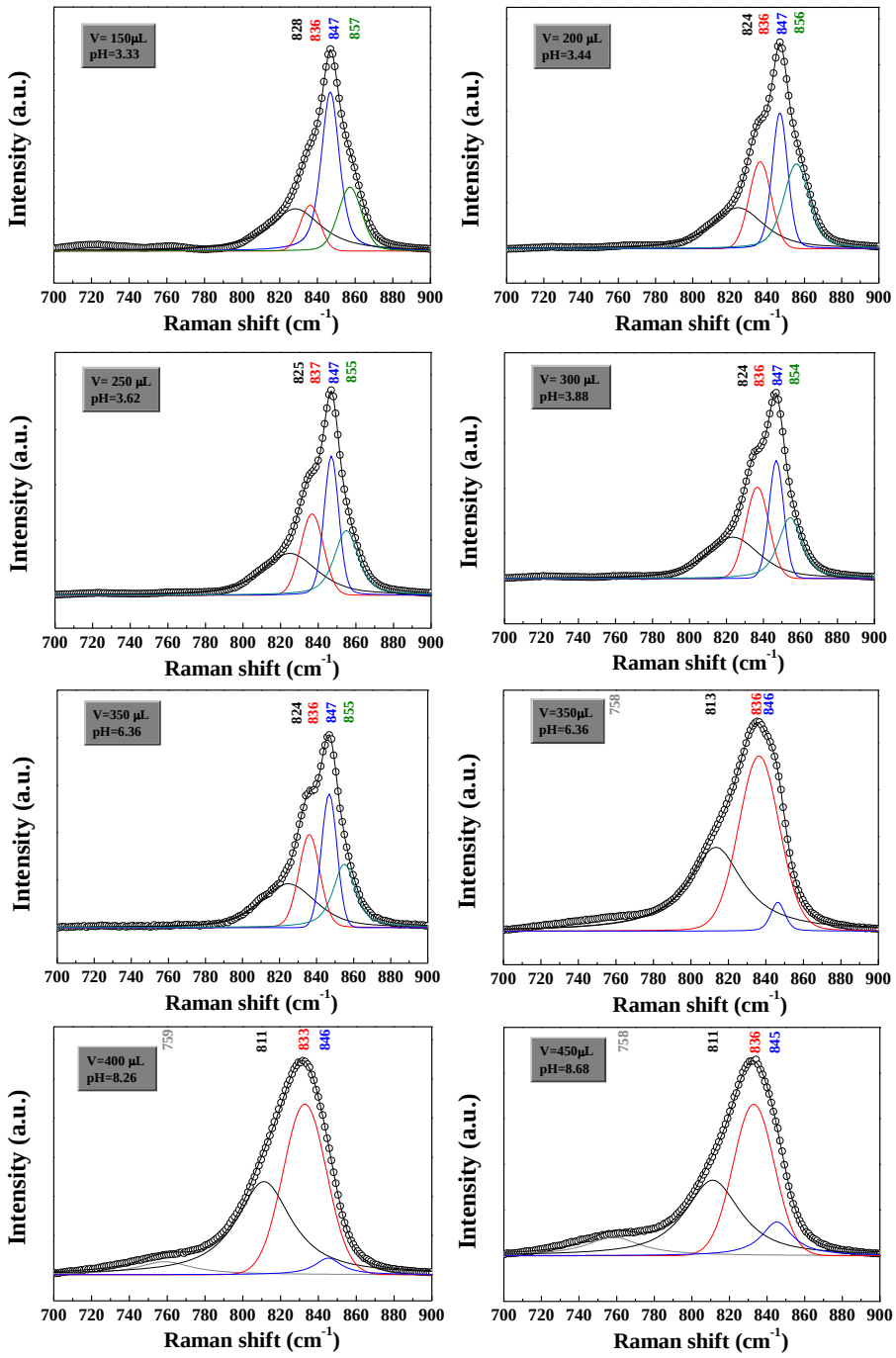

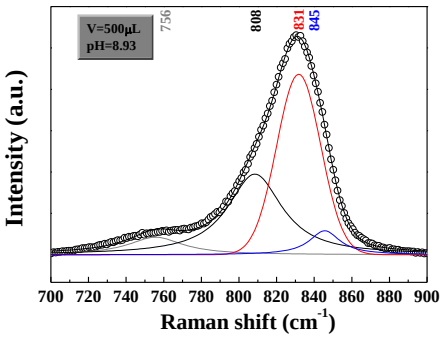

444
445
446 **Figure 12.** Raman profile analysis of the ADU precipitated by adding different amount
447 of NH_4OH.

448 **Table 2.** U-O distances for the found $\nu_s(UO_2^{2+})$, obtained by using the Bartlett and
449 Cooney relation [45].

	$\nu_s(UO_2^{2+})$ (cm^{-1}) / U-O bond length (Å)					
ADU$_B$	--	--	824/1.7867	836/1.7750	847/1.7646	855/1.7572
ADU$_C$	758/1.8560	811/1.7996				--

450

451 Figure 13 shows the variation of each band area as a function of the NH_4OH added and
452 we have also included the region A, B and C from Figure 7.B. Figure 13.A shows an
453 increase of Raman peak area of bands centered at 758, 811 and 836 cm^{-1} vs the volume
454 of NH_4OH added, which are higher in region C; whereas in Figure 13.B it is plotted the
455 area of the bands centered at ~828, 847 and 854 cm^{-1}, which decreases with the NH_4OH
456 added and are more abundant in region B. As can be seen, the comparison between areas
457 and regions obtained from the speciation diagram are in perfect agreement.
458 The precipitate ADU analysis by RS was compared with the extracted results from the
459 U(VI) speciation in the supernatant.

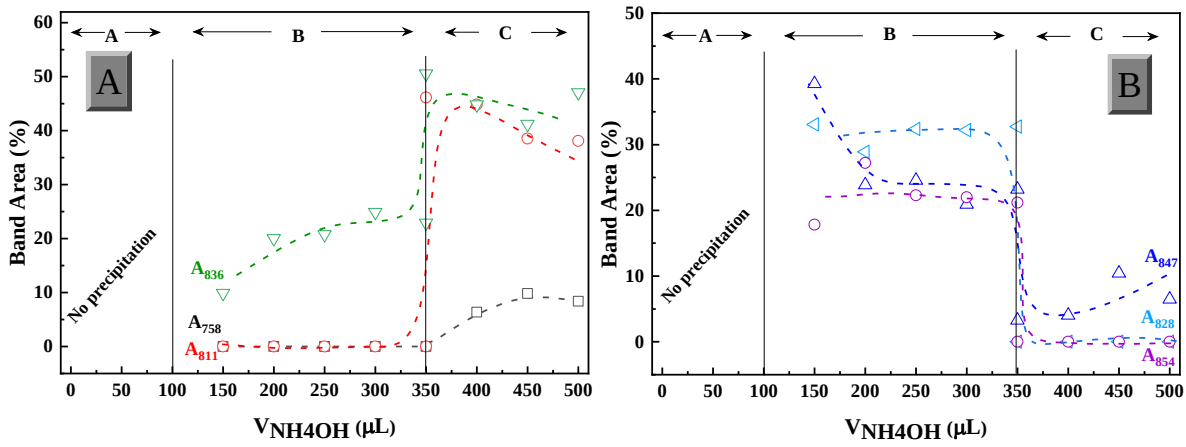

Figure 13. Results of the band profile analysis shown in Figure 12.

4. DISCUSSION

The described results can be interpreted in terms of the formation of hydroxo complexes $(UO_2)_x\ (OH)_y^{(2x-y)+}$ with stoichiometry *(x,y)*. The behavior exhibited by the different Raman features previously analyzed leads to the following conclusions:

1) Two uranyl species have been identified, the free uranyl ion *(1,0)*, UO_2^{2+}, and the *(2,2)* complex, $(UO_2)_2(OH)_2^{2+}$.
2) The relative abundance of each ion and the amount of precipitate formed versus added volume of NH_4OH and/or the solution pH leads to three regions in the phase diagram:
   (A) At volume addition of $NH_4OH \leq 100$ µL (pH ≤ 3.0). The concentration of free ion decreases continuously, whereas $(UO_2)_2(OH)_2^{2+}$ concentration increases up to a maximum; at this maximum the concentration of both species are similar and ~ 0.11 M. ADU concentration is almost negligible in this region.
   (B) From 100 to 300 µL of NH_4OH added (3.0 < pH ≤ 3.9), both ion concentrations decrease and ADU concentration increases exponentially.

(C) At >300 µL of NH_4OH added, (pH > 3.9), $[UO_2^{2+}]$ and $[(UO_2)_2(OH)_2^{2+}]$ are very low and the ADU concentration reaches a maximum and then keeps constant.

It is noteworthy that the behavior of the ADU concentration is very similar to the *(3,5)* complex (obtained with the NaOH addition instead of NH_4OH addition). Therefore, we have assigned in a first approximation this stoichiometry to the ion related to the ADU precipitation process.

We have characterized the solid by SEM, XRD and RS. The XRD patters analysis indicates that ADU obtained can be described by a combination of the compounds (II) $3UO_3\ NH_3\ 5H_2O$ and (III) $2UO_3\ NH_3\ 3H_2O$, and as the pH is increased (more NH_4OH added), the crystallinity of the solid is reduced and it has more ammonia content. Regarding the Raman results, two different Raman spectra can be distinguished, corresponding to the regions B and C respectively. These are referred to in this as ADU_B and ADU_C, respectively. The detailed analysis of the Raman data illustrates that the main Raman band $\nu_s(UO_2^{2+})$ shows an internal structure composed of 4 main contributions. In ADU_B these bands are centered at *ca.* 824, 836, 847 and 855 cm^{-1}, and in the ADU_C they are located at 758, 811, 836 and 847 cm^{-1}. The decrease in frequency in ADUc has been interpreted in terms of bonding strengths as the NH_4^+ content increase, *i.e.* the U-O bond length are longer for ADU with higher ammonia content, in agreement with XRD results.

5. CONCLUSIONS

In this work, an approach by Raman spectroscopic technique is presented to track the ADU precipitation reaction from uranyl nitrate solution by the addition of different amounts of ammonium hydroxide. The supernatant solution and solids were analyzed separately. Thus, jointly considering the results of the U(VI) speciation in the supernatant and the characterization of the ADU precipitated, it turns out that:

(i) The named region A for V_{NH4OH} < 100 μL, where the ion *(1,0)* [UO_2^{2+}] is the most abundant and no quantitative precipitation is found. This *(1,0)* ion is characterized with a symmetric stretching vibration $\nu_s(UO_2^{2+})$ band at *ca.* 870 cm^{-1}, and is the ion with shortest U-O bond length (the highest frequency), consistent with decreased hydration of the uranyl ion. In the region A, as the amount of NH_4OH increases, the *(1,0)* ion transforms to the *(2,2)* [$(UO_2)_2(OH)_2^{2+}$] ion, which has a U-O bond length higher ($\nu_s(UO_2^{2+})$ ~853 cm^{-1}), indicating increased hydration.

(ii) Region B indicates the beginning of quantitative precipitation. The precipitation starts when the complex *(2,2)* reaches its maximum concentration, at a volume addition of NH_4OH = 150 μL, (pH > 3). This is the point in which the hypothetical complex *(3,5)* [$UO_3(OH)_5^{4+}$] would be formed (see Figure 7A). Therefore, one can hypothesize that the solid ADU_B precipitated in this region are formed from the ions *(2,2)* and *(3,5).*

(iii) Region C, at V_{NH4OH} > 350 μL (pH > 6.36), the main solid analyzed could be formed from the *(3,5)* ion as the complexes concentration in the supernatant is almost negligible.

The comparison of the U-O bond length within the uranyl ions in the aqueous phase and the solid precipitates are in agreement with the previously exposed arguments. So, the U-O distance in the ADU_B solid is shorter than in the ADU_C, as was the case of the uranyl ion that is shorter for the *(2,2)* ion than for the *(3,5).*

Another valuable conclusion from this study is the major challenge for using the Raman spectroscopic technique as an alternative online technique, which can provide important information for the industrial UO_2 production when it is used for in-situ tracking the ADU precipitation reaction. This information about the quantitative and speciation of uranyl

ion can be used to control the normal and safe performance during the operation of these processes, which is one of the paramount issues for the manufacturing industry in nuclear power. Traditionally, this control is carried out by sampling the streams for the *ex-situ* analysis with different analytical techniques. These off-line techniques are destructive and incur significant costs and long test times. Therefore, we propose the use of *online* Raman spectroscopic technique for monitoring these species, mitigating the time-consuming of those protocols and the additional risk of operation with such a radioactive and hazardous material.

ACKNOWLEDGMENTS

This work was supported by AEI project MDM-546 2017- 0737 Unidad de Excelencia "María de Maeztu" and PGC2018-094814-B-C21 (Ministerio de Ciencia e Innovación). The authors also want to thank to Luis Gutiérrez and Sofía Durán for their help in the samples analysis by XRD and ICP-MS.

6. REFERENCES

[1] A. Blum, The manufacture of uranium dioxide fuel in pellet form, Israel, 1975, p. 13.

[2] C. Ganguly, U. Basak, Fabrication of high density UO2 fuel pellets involving sol-gel microsphere pelletisation and low temperature sintering, Journal of Nuclear Materials 178(2) (1991) 179-183.

[3] IAEA, Experiences and Trends of Manufacturing Technology of Advanced Nuclear Fuels, INTERNATIONAL ATOMIC ENERGY AGENCY, Vienna, 2012.

[4] A. Oliver, Refining/conversion and further processing of uranium concentrate. Short Course., 3rd International Conference On Uranium. 40th Annual Hydrometallurgy Meeting, Saskatoon, Saskatchewan, Canada, 2010.

[5] H. Roepenack, V.W. Schneider, W.G. Druckenbrodt, Experience with the AUPuC-conversion process for mixed oxide fuel fabrication, Journal of the American Ceramic Society Bulletin 63 (1984) 1051-1053.

[6] M. Peehs, T. Walter, S. Walter, M. Zemek, Uranium, Uranium Alloys, and Uranium Compounds, 2007.

[7] R.E. Lerch, R.E. Norman, Nuclear Fuel Conversion and Fabrication Chemistry, Radiochimica Acta 36(1-2) (1984) 75.

[8] P.V.S.N. Prudhvi Raju, D. Mandal, Study on the effect of free acidity and entrained TBP in UNPS on the quality of ADU powder, Journal of Nuclear Materials 464 (2015) 346-355.

[9] S. Manna, R. Kumar, S.K. Satpati, S.B. Roy, J.B. Joshi, Study of the changes in composition of ammonium diuranate with progress of precipitation, and study of the properties of ammonium diuranate and its subsequent products produced from both uranyl nitrate and uranyl fluoride solutions, Nuclear Engineering and Technology 49(3) (2017) 541-548.

568 [10] W.I. Stuart, T.L. Whateley, Composition and structure of ammonium uranates,
569 Journal of Inorganic and Nuclear Chemistry 31(6) (1969) 1639-1647.
570 [11] R. Eloirdi, D. Ho Mer Lin, K. Mayer, R. Caciuffo, T. Fanghänel, Investigation of
571 ammonium diuranate calcination with high-temperature X-ray diffraction, Journal of
572 Materials Science 49(24) (2014) 8436-8443.
573 [12] H. Doi, T. Ito, Significance of physical state of starting precipitate in growth of
574 uranium dioxide particles, Journal of Nuclear Materials 11(1) (1964) 94-106.
575 [13] J. Janov, P.G. Aijfredson, V.K. Vilkaitis, The influence of precipitation conditions
576 on the properties of ammonium diuranate and uranium dioxide powders, Journal Of
577 Nuclear Materials 44 (1972) 161-174.
578 [14] J.L. Woolfrey, The preparation of UO2 powder: Effect of ammonium uranate
579 properties, Journal of Nuclear Materials 74(1) (1978) 123-131.
580 [15] B. Narasimha Murty, P. Balakrishna, R.B. Yadav, C. Ganguly, Influence of
581 temperature of precipitation on agglomeration and other powder characteristics of
582 ammonium diuranate, Powder Technology 115(2) (2001) 167-183.
583 [16] S. Manna, S.B. Roy, J.B. Joshi, Study of crystallization and morphology of
584 ammonium diuranate and uranium oxide, Journal of Nuclear Materials 424(1) (2012) 94-
585 100.
586 [17] S. Paik, S. Biswas, S. Bhattacharya, S.B. Roy, Effect of ammonium nitrate on
587 precipitation of Ammonium Di-Uranate (ADU) and its characteristics, Journal of Nuclear
588 Materials 440(1) (2013) 34-38.
589 [18] B. Tomažič, M. Samaržija, M. Branica, Precipitation and hydrolysis of uranium (VI)
590 in aqueous solutions-VI: Investigation on the precipitation of ammonium uranates,
591 Journal of Inorganic and Nuclear Chemistry 31(6) (1969) 1771-IN2.

592 [19] K. Müller, V. Brendler, H. Foerstendorf, Aqueous Uranium(VI) Hydrolysis Species
593 Characterized by Attenuated Total Reflection Fourier-Transform Infrared Spectroscopy,
594 Inorganic Chemistry 47(21) (2008) 10127-10134.
595 [20] L.M. Toth, G.M. Begun, Raman spectra of uranyl ion and its hydrolysis products in
596 aqueous nitric acid, The Journal of Physical Chemistry 85(5) (1981) 547-549.
597 [21] M.H. Brooker, C.B. Huang, J. Sylwestrowicz, Raman spectroscopic studies of
598 aqueous uranyl nitrate and perchlorate systems, Journal of Inorganic and Nuclear
599 Chemistry 42(10) (1980) 1431-1440.
600 [22] L. Maya, G.M. Begun, A Raman spectroscopy study of hydroxo and carbonato
601 species of the uranyl (VI) ion, Journal of Inorganic and Nuclear Chemistry 43(11) (1981)
602 2827-2832.
603 [23] C. Nguyen Trung, G.M. Begun, D.A. Palmer, Aqueous uranium complexes. 2.
604 Raman spectroscopic study of the complex formation of the dioxouranium(VI) ion with
605 a variety of inorganic and organic ligands, Inorganic Chemistry 31(25) (1992) 5280-5287.
606 [24] M. Dargent, J. Dubessy, L. Truche, E.F. Bazarkina, C. Nguyen-Trung, P. Robert,
607 Experimental study of uranyl(VI) chloride complex formation in acidic LiCl aqueous
608 solutions under hydrothermal conditions (T = 21 °C–350 °C, Psat) using Raman
609 spectroscopy, European Journal of Mineralogy 25(5) (2013) 765-775.
610 [25] F. Quilès, A. Burneau, Infrared and Raman spectra of uranyl(VI) oxo-hydroxo
611 complexes in acid aqueous solutions: a chemometric study, Vibrational Spectroscopy
612 23(2) (2000) 231-241.
613 [26] G. Lu, T.Z. Forbes, A.J. Haes, Evaluating Best Practices in Raman Spectral Analysis
614 for Uranium Speciation and Relative Abundance in Aqueous Solutions, Analytical
615 Chemistry 88(1) (2016) 773-780.

[27] L.J. Bonales, I. Sánchez-García, Quantitative Raman Spectroscopy (QRS) for Nuclear Fuel Reprocessing Applications, LAP LAMBERT Academic Publishing 2020.

[28] P.J. Larkin, Chapter 3 - Instrumentation and Sampling Methods, in: P.J. Larkin (Ed.), Infrared and Raman Spectroscopy (Second Edition), Elsevier2018, pp. 29-61.

[29] B. Wopenka, J.D. Pasteris, Raman intensities and detection limits of geochemically relevant gas mixtures for a laser Raman microprobe, Analytical Chemistry 59(17) (1987) 2165-2170.

[30] G.E. Walrafen, M.S. Hokmabadi, W.H. Yang, Raman isosbestic points from liquid water, The Journal of Chemical Physics 85(12) (1986) 6964-6969.

[31] G.E. Walrafen, Raman Spectral Studies of Water Structure, The Journal of Chemical Physics 40(11) (1964) 3249-3256.

[32] M. Xu, J.P. Larentzos, M. Roshdy, L.J. Criscenti, H.C. Allen, Aqueous divalent metal–nitrate interactions: hydration versus ion pairing, Physical Chemistry Chemical Physics 10(32) (2008) 4793-4801.

[33] M.R. Waterland, D. Stockwell, A.M. Kelley, Symmetry breaking effects in NO3−: Raman spectra of nitrate salts and ab initio resonance Raman spectra of nitrate–water complexes, The Journal of Chemical Physics 114(14) (2001) 6249-6258.

[34] N.J. Mendoza, L.J. Bonales, V.G. Baonza, M. Cáceres, Local hydration pressures in methanol aqueous solution: a Raman spectroscopy analysis, The journal of physical chemistry. B 118(33) (2014) 9919-25.

[35] B.D. Cullity, S.R. Stock, Elements of X-ray Diffraction, Third Edition, Pearson, New York, 2001.

[36] P.C. Debets, B.O. Loopstra, On the uranates of ammonium—II: X-ray investigation of the compounds in the system NH3□UO3□H2O, Journal of Inorganic and Nuclear Chemistry 25(8) (1963) 945-953.

641 [37] E.H.P. Cordfunke, Composition and structure of ammonium uranates, Journal of
642 Inorganic and Nuclear Chemistry 32(9) (1970) 3129-3131.
643 [38] G. Lu, A.J. Haes, T.Z. Forbes, Detection and identification of solids, surfaces, and
644 solutions of uranium using vibrational spectroscopy, Coordination chemistry reviews 374
645 (2018) 314-344.
646 [39] L.J. Bonales, C. Menor-Salván, J. Cobos, Study of the alteration products of a natural
647 uraninite by Raman spectroscopy, Journal of Nuclear Materials 462 (2015) 296-303.
648 [40] F. Pointurier, O. Marie, Identification of the chemical forms of uranium compounds
649 in micrometer-size particles by means of micro-Raman spectrometry and scanning
650 electron microscope, Spectrochimica Acta Part B: Atomic Spectroscopy 65(9) (2010)
651 797-804.
652 [41] A. Berlizov, D.M.L. Ho, A. Nicholl, T. Fanghänel, K. Mayer, Assessing hand-held
653 Raman spectrometer FirstDefender RM for nuclear safeguards applications, Journal of
654 Radioanalytical and Nuclear Chemistry 307(1) (2016) 285-295.
655 [42] D.H.M. Lin, D. Manara, Z. Varga, A. Berlizov, T. Fanghänel, K. Mayer,
656 Applicability of Raman spectroscopy as a tool in nuclear forensics for analysis of uranium
657 ore concentrates, Radiochimica Acta 101(12) (2013) 779.
658 [43] D. Ho Mer Lin, D. Manara, P. Lindqvist-Reis, T. Fanghänel, K. Mayer, The use of
659 different dispersive Raman spectrometers for the analysis of uranium compounds,
660 Vibrational Spectroscopy 73 (2014) 102-110.
661 [44] D.M.L. Ho, A.E. Jones, J.Y. Goulermas, P. Turner, Z. Varga, L. Fongaro, T.
662 Fanghänel, K. Mayer, Raman spectroscopy of uranium compounds and the use of
663 multivariate analysis for visualization and classification, Forensic Science International
664 251 (2015) 61-68.

665 [45] J.R. Bartlett, R.P. Cooney, On the determination of uranium-oxygen bond lengths in
666 dioxouranium(VI) compounds by Raman spectroscopy, Journal of Molecular Structure
667 193 (1989) 295-300.